Off-resonant all-optical switching dynamics in a ferromagnetic model system

Christiane Scholl, Svenja Vollmar,* and Hans Christian Schneider†
Physics Department and Research Center OPTIMAS, Kaiserslautern University, P. O. Box 3049, 67663 Kaiserslautern, Germany

(Received 7 March 2018; revised manuscript received 21 April 2019; published 17 June 2019)

We present a theoretical study of the effects of optical fields on a ferromagnetic model system of itinerant carriers that includes both magnetism at the level of a time-dependent mean-field and spin-orbit coupling. In the framework of this model, which contains a band gap and is similar to the one introduced by Qaiumzadeh *et al.* [Phys. Rev. B **88**, 064416 (2013)] we investigate the inverse Faraday effect, i.e., how the magnetization of the ferromagnetic bands can be influenced by the helicity of off-resonant optical fields. The magnetization dynamics are calculated self-consistently by including a dynamic ferromagnetic splitting and the corresponding single-particle states. We study the magnetization dynamics for the case of a rapid ramping-up of an optical field that is off-resonant with respect to the gap and find that the magnetization switching occurs due to the interplay of the coherence between the spin-split ferromagnetic bands and incoherent scattering/dephasing processes.

DOI: 10.1103/PhysRevB.99.224421

I. INTRODUCTION

The optical excitation of magnetic systems has many facets that have been explored over the last two decades. After demagnetization of 3D ferromagnets by ultrashort pulses was discovered, it was realized that in alloys with antiferromagnetically coupled sublattices ultrafast magnetization dynamics occurs with the possibility of going through a transient ferromagnetic-like state [1] and may lead to magnetization switching, which can be understood in terms of transient heating effects [2–5]. More recently, there has also been evidence for magnetization switching induced in *ferromagnets* [6,7] where a purely heat-induced effect should not work. In the connection with ultrafast magnetism, the inverse Faraday effect (IFE) has been introduced as a possible candidate for a coupling of polarized optical fields to the magnetization that can be responsible for *all-optical* switching [8,9], that is, a switching process controlled directly by the helicity of the optical field and not due to heating effects. For a while, the IFE in ultrafast magnetism was envisaged phenomenologically as an additional B field [8,9], without clarifying the microscopic mechanism with which the polarized optical fields act on the magnetization. However, there has been an ongoing debate of what the important contributions to all-optical switching are and what the role of magnetic circular dichroism is [10–12].

The inverse Faraday effect, which was investigated in the 1960s [13,14] for nonmagnetic, nonabsorbing systems. These early quantum-mechanical analyses relied on an effective potential that is strictly valid only in equilibrium but are still in use [15]. There have also been papers that stress the interaction of ferromagnets with classical fields [16–19], which is outside the scope of this paper. Gridnev [20] has analyzed the switching behavior of the magnetization in an s-d model considering essentially a heat-induced mechanism without taking into account the microscopic details of the matter-field interaction. Other authors investigated light-matter interactions that do not explicitly refer to ferromagnetic switching. [21–23]

For the purpose of discussing the results of the present paper, by way of comparison or contrast, we mention the following approaches to the inverse Faraday effect. In semiconductors, such as GaAs and CdMnTe, the so-called specular IFE has been measured using picosecond pulses and explained by the spin-selective absorption of polarized optical fields and subsequent spin relaxation [24]. Because of the important role of incoherent absorption the specular IFE is not an off-resonant effect. In Refs. [25,26] stimulated spin-flip Raman scattering of photons was analyzed using time-dependent quantum-mechanical calculations for few-level systems. In this case, the field was assumed to be resonant with intermediate levels and the angular momentum needed for the switching is transferred from the field via a spin-flip Raman process. Qaiumzadeh *et al.* [27] analyzed the IFE in nonmagnetic and magnetic semiconductor models using the second-order perturbation theory approach of Pershan *et al.* [14]. Following Shen [28], Qaiumzadeh *et al.* call it the spin-selective optical Stark effect. The stationary perturbation calculation in Ref. [27] does not explicitly include magnetization dynamics, but the authors stress that the actual magnetization change has to occur by spin-flip transitions of electrons between the magnetically split bands, for which the spin-orbit coupling would be responsible [14,27]. This is an important aspect of their approach as the change in spin angular momentum that accompanies helicity-dependent switching arises from spin-orbit coupling and is not transferred from photons. For band ferromagnets, a second-order perturbation theory approach to the IFE based on *ab initio* matrix elements has only recently been introduced in Refs. [29,30]. Here, the induced magnetization due to the optical fields is calculated. While this approach has been successfully combined with classical spin models to describe the magnetization

*Graduate School of Excellence Materials Science in Mainz, Gottlieb-Daimler-Strasse 47, 67663 Kaiserslautern, Germany.
†hcsch@physik.uni-kl.de

dynamics, a drawback of this approach is that the "intrinsic" magnetization dynamics is not calculated self consistently with the spin-dependent effects introduced by the optical fields [7].

The present paper theoretically analyzes magnetization dynamics in a ferromagnetic model system that, as we show, exhibits all-optical switching by off-resonant fields, which constitutes the IFE. The model system contains itinerant electrons, exhibits a ferromagnetic splitting and has a gap. Our dynamical calculation is self-consistent in the sense that when the polarization of the magnetic system is changed by the optical field and incoherent electronic scattering processes, the system properties (states and quasiparticle energies) are changed. This allows us to investigate, in one comprehensive microscopic model, the complete magnetic switching process due to polarized optical fields in which the system reaches a switched state. We also note that incoherent electronic scattering processes cannot be classified in orders of the optical field, and our approach is nonperturbative in the optical field. This requires a relatively simple model band structure, for which we can determine the ferromagnetic state using a time-dependent mean-field approximation, and the first requirement means that we consider in our model also bands that are energetically removed by a band gap from the "magnetic" bands, but also dipole coupled to them. With these requirements, we end up with a microscopic, dynamical model for the IFE, described in Sec. II, that has important aspects in common with the ferromagnetic semiconductor considered by Qaiumzadeh [27] or the system considered by Li and Haney [31] to investigate optical spin torques and spin-orbit torques, albeit with a fixed magnetic splitting [31].

Compared to recent *ab initio* based approaches to magnetic materials [30,32], our band structure is does not describe a band ferromagnet or local magnetic correlations, [33] but is closer to a magnetic semiconductor or perovskite Rashba semiconductor [31]. However, our approach contributes to the conceptual understanding of the inverse Faraday effect, as the simplicity of the band structure used in this paper is offset by our calculation of the "self-consistent" magnetization dynamics and the inclusion of incoherent scattering mechanisms. Our results should also have some bearing on the interaction of polarized fields with magnetic dielectrics such as YIG. In difference to any second-order perturbation theory with respect to the field, we can follow the whole switching process including the self-consistent change of the ferromagnetic splitting. The inclusion of incoherent redistribution processes means that this model can reach a driven steady state or a new equilibrium after the switching process.

The paper is organized as follows. We introduce the model and the dynamical equations for the reduced density matrix in Sec. II, where we also explain our relaxation-time ansatz used for the incoherent redistribution of carriers. In Sec. III, we discuss results of dynamical calculations for a parabolic band structure (without spin-orbit coupling) and for the ferromagnetic Rashba band structure. We discuss the features of the magnetization dynamics and compare with previous pictures of the IFE in Refs. [27,34]. Our conclusions are contained in Sec. IV.

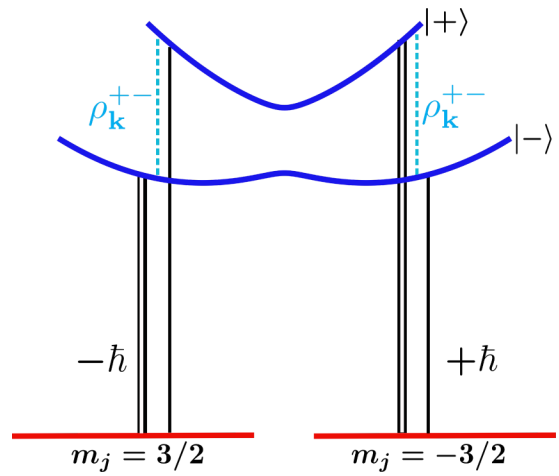

FIG. 1. Schematic structure of the four-band system with two magnetically split conduction bands separated from two filled valence bands by a gap. Dipole transitions between the valence and conduction bands are shown for a few k points schematically by vertical lines. The coherence ρ^{+-} between the magnetic bands is also shown. Note that we do not show the k dependence of the valence bands and plot them side by side instead of on top of each other. The different dipole coupling matrix elements are indicated by the thickness of the arrows and the angular momentum transferred to the carriers by a left (right) circularly polarized photon is indicated by $-\hbar(+\hbar)$. Both $|+\rangle$ and $|-\rangle$ states are connected to each of the p-like states by dipole transitions with both helicities.

II. MODEL

In this section, we describe the band structure of our ferromagnetic model system and present the dynamical equations for the coherent and incoherent processes that affect the electrons in the magnetic bands.

A. Ferromagnetic model system

The band structure for the electronic states is sketched in Fig. 1. It combines two spin-split bands $|\pm, \mathbf{k}\rangle$ of a ferromagnetic Rashba system, as described in Ref. [35], and two filled parabolic bands. The band structure is somewhat similar to the models used by Qaiumzadeh *et al.* [27], and in that it possesses a band gap separating conduction and valence bands. We refer to the valence bands as hole bands for clarity, but the magnetic splitting, which is of primary interest in this paper, is due to a Stoner mean field in the electronic Rashba bands. While the hole bands are p-like, we include only heavy holes such that there is no direct spin mixing in the hole bands. The Rashba spin-orbit contribution introduces a spin mixing in the magnetically split electronic bands. There is no contribution from holes and/or magnetic impurities to the magnetism. In Ref. [27], only the p-like hole bands are spin mixed due to spin-orbit coupling and in Ref. [31] both electron and hole bands are spin mixed. As mentioned in Sec. I, this system does not describe a real material, but is designed to contain the essential ingredients for the occurence of an inverse Faraday effect, notably spin-orbit coupling [14,25], electronic scattering processes and a ferromagnetic exchange splitting that can change in response to the electronic

dynamics. The simplicity of the band structure makes it possible to calculate the electronic dynamics and the corresponding magnetization dynamics self-consistently by taking into account the time-dependent magnetic properties and the concomitant change of the band structure. Electronic scattering processes in connection with the spin-orbit coupling play a decisive role in the electronic spin dynamics [35] and are therefore crucial for a correct description of the self-consistent magnetization dynamics.

We first discuss the band structure shown schematically in Fig. 1 in some more detail. The two partially filled s-like bands $|\pm, \mathbf{k}\rangle$ exhibit a magnetic splitting of about 20 meV due to a Stoner mean-field contribution but also include spin-orbit coupling. They are dipole coupled to two hole bands $|\pm\frac{3}{2}\rangle$, which are modeled as filled p-like bands with total angular momentum $j = 3/2$, $l = 1$, and $m_j = \pm 3/2$ [36]. The band gap is large compared to the equilibrium magnetic splitting and amounts to 1.5 eV for $\mathbf{k} = 0$. We use a Rashba-type spin-orbit coupling with an effectively two-dimensional k space and include magnetism at the level of a Stoner splitting

$$\hat{H} = \begin{pmatrix} \frac{\hbar^2\mathbf{k}^2}{2m^*} + \frac{U}{2}(n-m) & -\alpha(k_y + ik_x) \\ \alpha(-k_y + ik_x) & \frac{\hbar^2\mathbf{k}^2}{2m^*} + \frac{U}{2}(n+m) \end{pmatrix}, \tag{1}$$

where $n = \sum_{\mathbf{k}} \sum_{\mu=\pm} \rho_{\mathbf{k}}^{\mu\mu}$ denotes the particle density in the magnetic bands and is calculated as the trace of the density operator, whereas

$$m = \sum_{\mathbf{k}} \langle \sigma_z(\mathbf{k}) \rangle = \sum_{\mathbf{k},\mu,\mu'=\pm} \langle \mu, \mathbf{k} | \sigma_z | \mu', \mathbf{k} \rangle \rho_{\mathbf{k}}^{\mu,\mu'} \tag{2}$$

represents the spin polarization per site in the magnetic bands, which is as well determined from the reduced spin density matrix. The Stoner exchange splitting is $\Delta = Um$, and the magnetic and spin-orbit splitting are controlled, respectively, by the Stoner and Rashba parameters U and α. While the carrier densities and splitting are smaller than in metallic ferromagnets, the effective Hamiltonian (1) allows one to determine the band structure in a "self-consistent" fashion as the effective Hamiltonian depends on the spin splitting and the spin splitting depends on the single-particle eigenstates of the effective Hamiltonian. In the time-dependent calculation, we use the instantaneous distributions to determine the instantaneous eigenstates. Using the instantaneous eigenstates and the instantaneous splitting has been shown to be important for "heat-induced" magnetization dynamics in ferromagnetic model systems [37,38].

The magnetic equilibrium state before the interaction with the optical fields is determined self-consistently from Eqs. (2) and (1). The Rashba Hamiltonian with additional magnetic contributions results in band energies

$$\epsilon_{\pm}(\mathbf{k}) = \frac{\hbar^2\vec{k}^2}{2m^*} + \frac{Un}{2} \pm \sqrt{\alpha^2 k^2 + \left(\frac{Um}{2}\right)^2}, \tag{3}$$

The eigenstates, see, e.g., Ref. [35], are nonpure spin states, which we denote by $|\Uparrow\rangle = |-\rangle$ for the lower and $|\Downarrow\rangle = |+\rangle$ for the upper Rashba band, so the resulting spin polarization in z direction is positive in the equilibrium magnetic state. The spin operator σ_z is not diagonal in the basis of the Rashba Hamiltonian, which results in a characteristic spin structure. Last, the hole bands are considered to be parabolic bands filled with charge carriers, and their wave functions are assumed to be $\mathbf{k}$ independent.

The magnetization dynamics are induced by the coupling to the optical field via dipole matrix elements connecting the magnetic electron bands and the hole bands, as shown in Fig. 1. The Rashba spin mixing in the magnetic states means that each helicity state of the optical field couples both magnetic bands to a common p-like state. Note that in the approach of Qaiumzadeh *et al.* [27], the spin-orbit coupling was contained in the light-hole states, but not in the electronic states. The asymmetry between opposite circular field polarizations arises from the different strengths of the dipole matrix elements between the magnetic states and p-like states, as indicated in Fig. 1.

B. Dynamics of the reduced density matrix

We describe the coherent dynamics of the four band system sketched in Fig. 1 using the reduced single-particle density matrix $\rho_{\mathbf{k}}^{\mu\nu} = \langle \hat{c}_{\mathbf{k},\nu}^{\dagger} \hat{c}_{\mathbf{k},\mu} \rangle$, where $\hat{c}_{\mu,\mathbf{k}}^{\dagger}$ creates a particle in a Bloch state labeled by band index μ, which runs over the four bands shown in Fig. 1, and crystal momentum $\mathbf{k}$:

$$\frac{\partial}{\partial t}\rho_{\mathbf{k}}^{\nu\mu} = \frac{i}{\hbar}(\epsilon_{\mu}(\mathbf{k}) - \epsilon_{\nu}(\mathbf{k}))\rho_{\mathbf{k}}^{\mu\nu} - \frac{i}{\hbar}\sum_{\mu'}\left[\rho_{\mathbf{k}}^{\nu\mu'}\Omega_{\mathbf{k}}^{\mu',\mu}(t) - \Omega_{\mathbf{k}}^{\nu,\mu'}(t)\rho_{\mathbf{k}}^{\mu'\mu}\right] + \frac{\partial}{\partial t}\rho_{\mathbf{k}}^{\mu\nu}\Big|_{\text{scat}}. \tag{4}$$

Here, $\hbar\Omega_{\mathbf{k}}^{\mu\nu}(t) = \mathbf{d}_{\mu,\nu}(\mathbf{k}) \cdot \mathbf{E}(t)$ are the matrix elements of the Rabi frequency (or Rabi energy, as it is commonly called in semiconductor optics), which contains the electric field vector $\mathbf{E}(t)$ and the matrix elements of the dipole operator $\mathbf{d} = -e\mathbf{r}$. For our choice of basis states, only certain matrix elements are nonzero. Using the notation $\vec{\sigma}_{\pm} = (\mathbf{e}_x \pm i\mathbf{e}_y)/\sqrt{2})$ these are, without Rashba spin-orbit coupling in the electronic states, $\langle\uparrow|\mathbf{d}|m_j = 3/2\rangle = d_0\vec{\sigma}_{+}$ and $\langle\downarrow|\mathbf{d}|m_j = 3/2\rangle = d_0\sigma_{-}$, with equal magnitude $|d_0| = e5$ Å, which is taken as a parameter in $k \cdot p$ theory. Including the Rashba spin-orbit coupling in the electronic bands leads to four nonzero matrix elements $\langle\pm|\mathbf{d}|m_j = \pm 3/2\rangle$, two of which are weaker due to the relative smallness of the spin-orbit coupling. These dipole allowed transitions are shown as lines in Fig. 1 with the line thickness indicating their relative strengths. Due to the magnetic splitting in the electron bands, there is an asymmetry in the coupling to the different helicities of the optical field, but there is no dipole matrix element between the magnetic bands. Note that we work in the following with real-valued fields with circular polarization of the form $\vec{E}(t) = \cos(\nu t)\mathbf{e}_x \pm \sin(\nu t)\mathbf{e}_y$, which include photon states with both helicities, so that right and left circular polarized fields couple to transitions with both helicities, $+\hbar$ and $-\hbar$. In absorption, these dipole matrix elements would give rise to circular dichroism, which plays an important role in heat-induced magnetic switching phenomena [39]. Note that, in addition to the spin-orbit coupling of Rashba type in the electronic bands, the model includes spin-orbit coupling in the valence bands, which gives rise to the above-mentioned dipole matrix elements $\langle\uparrow|\mathbf{d}|m_j = 3/2\rangle = d_0\vec{\sigma}_{+}$ and $\langle\downarrow|\mathbf{d}|m_j = 3/2\rangle = d_0\sigma_{-}$. In the following, we will

have effects due to the valence band spin-orbit coupling alone, if we switch off the Rashba spin-orbit contribution. In this case, angular momentum changes in the system will be due to the coupling to the electromagnetic field alone. This effect is referred to as optical spin-transfer torque in Ref. [31]. When we include the Rashba spin-orbit coupling, we introduce a k-dependent spin mixing or noncollinearity, which gives rise to the possibility of an electronic spin dynamics not directly related to angular momentum transfer by the optical field. A similar contribution is called optical spin-orbit torque in Ref. [31], which also draws attention to the fact that here the lattice acts as a source or sink of angular momentum.

It is an important feature of Eq. (4) that the band energies $\epsilon_\mu(\mathbf{k})$ and basis states $|\mu, \mathbf{k}\rangle$ used for the matrix elements are the instantaneous eigenenergies of the mean-field Hamiltonian (1). In each time step, we use the basis of single particle states $|\mu, \mathbf{k}\rangle$ corresponding to the instantaneous values of n and m. This procedure includes the influence of the coherent optical field and the change of the instantaneous quasiparticle band structure via incoherent redistribution and relaxation processes, which we discuss next.

An important difference of the model band structure introduced here from that used by Qaiumzadeh *et al.* is that the spin orbit coupling is in the spin-split electronic states where it can be converted into electronic spin dynamics by spin-independent electronic scattering processes [35]. To model this redistribution of carriers for the magnetic electron bands, we introduce scattering contributions to the dynamical equations (4) for those elements of the reduced density matrix that describe the electronic system, namely, $\rho^{\mu\nu}$ with $\mu, \nu = \pm$, in the form of a relaxation-time ansatz. This ansatz models electron-electron scattering in (4) as a spin-independent scattering process in the following way:

$$\left.\frac{d\rho_{\mathbf{k}}^{\mu\nu}}{dt}\right|_{\text{scat}} = -\frac{\rho_{\mathbf{k}}^{\mu\nu} - \tilde{\rho}_{\mathbf{k}}^{\mu\nu}}{\tau}. \tag{5}$$

Here, $\tilde{\rho}_{\mathbf{k}}^{\mu\nu}$ indicates the elements of a suitably determined quasi-equilibrium spin density matrix.

In order to specifically model electron-electron scattering, we determine $\tilde{\rho}$ such that the relaxation-time ansatz conserves spin polarization, energy density and charge density of the carriers in the essential bands. The quantity τ is the effective scattering time for the incoherent electron-electron scattering. The spin polarization of the magnetic bands, which we take as the magnetization, is calculated via $\mathbf{m} = \sum_{\mathbf{k},\nu,\nu'} \langle \nu, \mathbf{k}|\vec{\sigma}|\nu', \mathbf{k}\rangle \rho_{\mathbf{k}}^{\nu\nu'}$ and includes the time-dependent spin expectation values of the eigenstates $|\nu, \mathbf{k}\rangle$ of (1).

The Bloch equations (4) are written using an index notation for the density matrix elements, formally including coherences between all bands, i.e., magnetic electron bands and hole bands. Here, we stress a particular contribution, namely, the coherence

$$\begin{aligned}\frac{\partial}{\partial t}\rho_{\mathbf{k}}^{+,-} &= \frac{i}{\hbar}(\epsilon_{\mathbf{k}+} - \epsilon_{\mathbf{k}-})\rho_{\mathbf{k}}^{+,-} \\ &+ \frac{i}{\hbar}\left(\Omega_{\mathbf{k}}^{+,-3/2}\rho_{\mathbf{k}}^{-3/2,-} - \rho_{\mathbf{k}}^{+,-3/2}\Omega_{\mathbf{k}}^{-3/2,-}\right. \\ &\left. + \Omega_{\mathbf{k}}^{+,3/2}\rho_{\mathbf{k}}^{3/2,-} - \rho_{\mathbf{k}}^{+,3/2}\Omega_{\mathbf{k}}^{3/2,-}\right),\end{aligned} \tag{6}$$

where the indices $m_j = \pm 3/2$ refer to the $j = 3/2$ valence band states, and $\pm$ labels the electronic states including Rashba and Stoner coupling. At each k, the electron-hole coherence corresponding to transitions of a given helicity and the coherence $\rho_{\mathbf{k}}^{+,-}$, forms a three-level system, as sketched in Fig. 1. In the theory of optically driven few-level systems, such a coherence is sometimes called a "quantum coherence" [40], or in spintronics, a spin coherence [41]. It is driven in second order of the field as can be seen from Eq. (6): both the Rabi energy and the polarizations between valence and conduction bands are first order in the E field. These terms involve photons of the same helicity, so that it is fundamentally different from the process studied by Popova *et al.* [26]. What we describe here in terms of the dynamical quantum coherence is related to the occurrence of an effective interaction Hamiltonian between different spin states calculated to second order in the field by Qaiumzadeh *et al.* [27]. It is also related to contributions in second order to the field that connect different spin states in the calculation of the induced magnetization performed by Berritta *et al.* [30]. These contributions are respectively interpreted as spin-selective optical Stark effect in Ref. [27] and Raman-type contributions in Ref. [30]. In the framework of the dynamical density matrix calculation, it is more natural to interpret the field driven quantum coherence as a spin expectation value at each k point that deviates from the direction of the effective spin-orbit field at this k point. [35] Note that the relaxation time ansatz provides also a dephasing contribution for the $\rho^{+,-}$ coherence. In the absence of spin-orbit coupling in the electron bands, no quantum coherence occurs.

To complete the discussion of the dynamical equations (4), we note that in addition to the quantum coherence (6) there are dynamical equations for the electronic distributions in the spin-split Rashba bands that are of the form

$$\begin{aligned}\frac{\partial}{\partial t}\rho_{\vec{k}}^{+,+} &= -\frac{i}{\hbar}\left(\rho_{\vec{k}}^{+,3/2}\Omega_{3/2,+}(\vec{k}) - \Omega_{+,3/2}(\vec{k})\rho_{\vec{k}}^{3/2,+}\right. \\ &\left. + \rho_{\vec{k}}^{+,-3/2}\Omega_{-3/2,+}(\vec{k}) - \Omega_{+,-3/2}(\vec{k})\rho_{\vec{k}}^{-3/2,+}\right)\end{aligned} \tag{7}$$

and, analogously,

$$\begin{aligned}\frac{\partial}{\partial t}\rho_{\vec{k}}^{-,-} &= -\frac{i}{\hbar}\left(\rho_{\vec{k}}^{-,3/2}\Omega_{3/2,-}(\vec{k}) - \Omega_{-,3/2}(\vec{k})\rho_{\vec{k}}^{3/2,-}\right. \\ &\left. + \rho_{\vec{k}}^{-,-3/2}\Omega_{-3/2,-}(\vec{k}) - \Omega_{-,-3/2}(\vec{k})\rho_{\vec{k}}^{-3/2,-}\right).\end{aligned} \tag{8}$$

While these equations contain contributions that arise from spin-orbit coupling in the electron bands, i.e., those due to dipole matrix elements shown as thin lines in Fig. 1, they also contain field induced effects in the absence of spin-orbit coupling in the electron bands. For clarity, we show those transitions that occur without Rashba spin-orbit coupling in the electronic states in a separate sketch in Fig. 2. When the Rashba parameter is set to 0, the bands become pure spin states of parabolic shape that are shifted in energy by the mean-field Stoner splitting. Even without Rashba SOC, in the case of uncoupled two-level systems at each k, the E field gives rise to a spin-dependent effect via Eqs. (7) and (8).

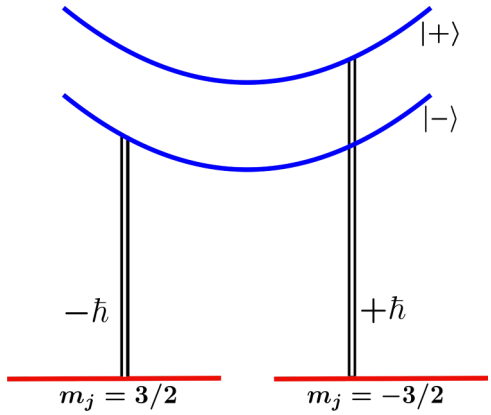

FIG. 2. Schematic structure of the four-band system without Rashba SOC: two magnetically split conduction bands are separated from two filled valence bands by a gap. Dipole transitions between the valence and conduction bands are shown for a few k points schematically by vertical lines. As there are no coherences $\rho^{+,-}$, at each k point, we have effectively uncoupled two-level systems.

III. RESULTS

The effects of the optical fields on the ferromagnet are calculated dynamically starting from an equilibrium state, which is determined self-consistently for the model Hamiltonian (1) and yields an initial magnetization, i.e., spin polarization, in $+z$ direction. In more detail, this is achieved for a given particle density and temperature as follows. The equilibrium distributions are assumed to be Fermi functions with the same chemical potential for both Rashba bands, which is determined self-consistently. In the chemical potential calculation, we simultaneously adjust the band structure including the magnetic splitting, which results in a spin-polarized state.

For the calculations presented here, we assume a Stoner parameter of $U = 50$ meV, a Rashba parameter of $\alpha = 20$ meV nm, a reduced mass of $m^* = m_e$ for the conduction bands, and a equilibrium temperature for the mean-field equilibrium calculation of $T = 70$ K. The reduced mass of the valence bands is $0.5\,m_e$, and we use a k cutoff of 9 nm^{-1}. For the effective electron-electron scattering time we take $\tau = 50$ fs. The self-consistent calculation for the magnetic equilibrium state yields an equilibrium spin polarization of 35%. Starting from this equilibrium state, we compute the dynamical distribution functions and states by solving (4) together with Eq. (1).

We study the effects of the switch-on of a circularly polarized optical pulse which is ramped up with a rise time of 40 fs at $t = 0$ and has an amplitude corresponding to a Rabi energy of $\hbar\Omega = 15$ meV for the transition $m_j = |3/2\rangle \rightarrow |\uparrow\rangle$ from which all k dependent matrix elements for the Rabi energies can be obtained. This Rabi energy corresponds to an intensity of 27 MW/cm^{-2}. The transitions at a fixed k are sketched as vertical lines in Fig. 1. As we are interested in the dynamics due to an off-resonant optical excitation, we take the frequency of the optical field to be detuned by 200 meV from the gap, which we measure from the top of the valence band to the minimum of the lower conduction band.

We assume a vanishing dephasing contribution, i.e., $d\rho^{\mu\nu}/dt|_{\rm scat} \equiv \gamma \rightarrow 0$ for the off-diagonal elements of the density matrix corresponding to the optical transitions across the gap, which is well justified for a large detuning [36].

We study here the dynamics due to off-resonant optical fields which create coherently driven carrier distributions using a simple switch-on scenario for the E field, instead of a sequence of pulses [42]. While in band ferromagnets resonant transitions and irreversible absorption most likely play a role [42], off-resonant interactions with optical fields are believed to be responsible for the microscopic mechanism of the inverse Faraday effect. Furthermore, an optical field can only be close to a resonance in some parts of k space in the band structure of a realistic d-band ferromagnet because of the very different curvatures of sp and d bands. In *ab initio* calculations with a relatively coarse k grid, the resonance condition is usually softened by an effective energy broadening in excess of 100 meV while still describing off-resonant effects in large parts of the Brillouin zone. In our model band structure, however, the electron and hole band curvatures are not very different and our resolution in k space is high, so that we work with a vanishing broadening for our investigation of off-resonant field effects [30].

In the following, we first focus on results without Rashba spin-orbit coupling in the electronic bands. As mentioned before, in this case only angular momentum exchange with the optical field is possible, which makes this scenario reminiscent of the optical spin-transfer torque [31]. Then we discuss in some details the switching dynamics including Rashba spin-orbit coupling, where the lattice can act as a source or sink of electronic spin angular momentum during the switching process.

A. Dynamics without Rashba SOC

We first discuss the system dynamics for the case *without* Rashba spin-orbit contributions in the electronic band structure. Apart from its importance for the optical spin-transfer scenario, it also establishes a test case for comparison with results including Rashba spin-orbit coupling below. The band structure and the relevant transitions for this case are shown in Fig. 2. We solve the dynamical equations (4) and include the dynamical Stoner gap determined from the instantaneous density matrix according to Eq. (2). Importantly, without Rashba SOC the there is no dynamical Eq. (6). In Fig. 3(a), we show the spin polarization (magnetization), for the excitation conditions discussed above. In addition to the magnetization, we characterize the electronic dynamics by means of the total energy density

$$e = \sum_{\mathbf{k}\mu} \epsilon_{\mathbf{k}\mu} \rho^{\mu\mu}_{\mathbf{k}} + U n_\uparrow n_\downarrow \tag{9}$$

in Fig. 3(b). We find that the spin polarization is lowered by right circular polarization and enhanced by the left-circular polarization of the optical field. The effect is small, less than 1%, but does not have the same magnitude for the two polarizations because of an asymmetry of the relevant transitions shown in Fig. 2. For right-circularly polarized light, which couples mainly to the transition $|m = -3/2\rangle \rightarrow |+\rangle \equiv |\downarrow\rangle$ the magnetization change is somewhat more pronounced because there are more empty states in the minority $|+\rangle$ band, which makes the coupling to this channel more efficient. This

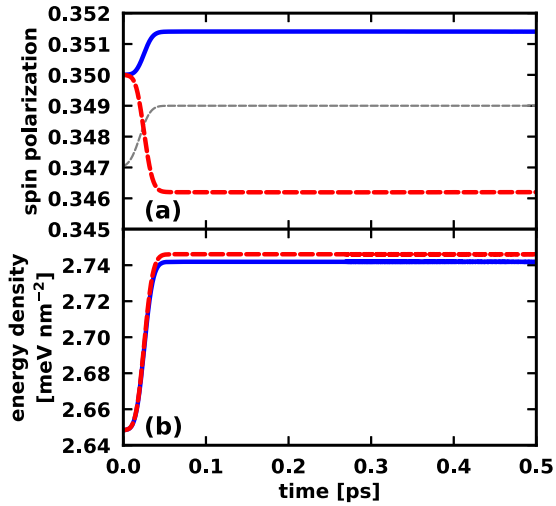

FIG. 3. (a) Time dependent magnetization (spin polarization) of the ferromagnetic model system *with parabolic bands* (no spin-orbit coupling in magnetic bands, no quantum coherence) excited by an optical field with right-circular (dashed line) and left-circular (solid line) polarization. The intensity of the driving field is shown, in arbitrary units, as thin grey dashed line. (b) Corresponding energy density.

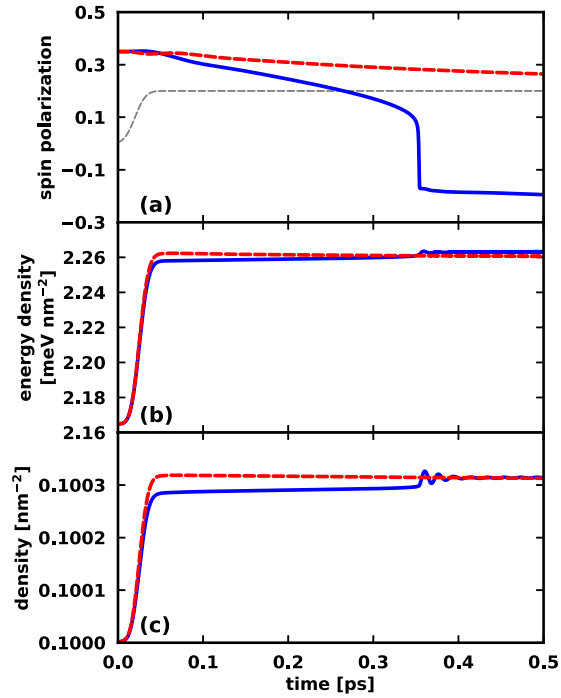

FIG. 4. (a) Time-dependent magnetization (spin polarization) of the ferromagnetic model system excited by a optical field with right-circular (dashed line) and left-circular (solid line) polarization. Magnetization switching occurs only for left-circularly-polarized excitation. (b) corresponding energy density. (c) corresponding density.

transition changes the angular momentum of the electron plus hole system by $+\hbar$ per photon, but because it couples to the $|+\rangle = |\downarrow\rangle$ band, the magnetization is reduced for right-circularly polarized light. For the left-circular excitation, the transition couples to the majority band $|-\rangle = |\uparrow\rangle$ where there are fewer final states, and we observe a smaller effect in the opposite direction, i.e., the magnetization is enhanced slightly.

We can gauge the influence of the electromagnetic field on our magnetic model system from the energy density plot, which also shows an increase of about 5% for both circular polarizations. The influence on the spin polarization occurs only on the short time scale on which the intensity of the optical field changes. Only then there are spectral components of the field that can lead to dipole transitions in the system. Since we neglect dephasing in the electron-hole polarizations here, the excited carrier distributions are completely coherent.

Without Rashba spin-orbit coupling in the electronic states, there is no quantum coherence contribution (6) in the dynamics shown in Fig. 3 because the driving terms to second order in the field are zero as there are no dipole moments for the $+3/2 \rightarrow \downarrow$ and $-3/2 \rightarrow \uparrow$ transitions. As we do not include an explicitly spin-dependent interaction, the vanishing of the quantum coherence entails that there are no scattering transitions that lead to a change in the ensemble spin, as a scattering mechanism has to be combined with the quantum coherence dynamics to lead to effective spin-flip transitions, if one uses the full electronic density matrix [35]. In this calculation without SOC in the electron bands, Eqs. (8) and (7) lead to a spin-dependent effect because the resonance condition for the field and the occupations are different for the $|\uparrow\rangle$ and $|\downarrow\rangle$ bands, as discussed above. The magnetization dynamics in Fig. 3 is thus somewhat similar to the mechanism for inverse Faraday effect measured and analyzed in semiconductors by Zheludev and coworkers [24] for resonant excitation. In their case, the real absorption of photons of different helicity leads to excited electrons with opposite spin due to the dipole selection rules between electron and hole bands and the available phase space for the transitions.

B. Dynamics with Rashba SOC

In Fig. 4, we turn to the field induced dynamics computed for the model of Eq. 1 including Rashba spin-orbit coupling and dynamical Stoner mean-field splitting. We keep the same excitation conditions, i.e., we ramp the optical field up over 40 fs. Figure 4(a) shows the time-dependent magnetization for off-resonant optical fields with right- and left-circular polarization. For the left-polarized optical field the magnetization is reduced to about 1/4 of its initial value during about 200 fs, and then the magnetization direction is reversed rapidly in about 50 fs. After the magnetization has switched its sign at about 250 fs, there is a much slower decay of the magnetization. For right-polarized light, we find in Fig. 4(a) essentially only demagnetization. Comparison of the magnetization dynamics for the two light polarizations shows that this model ferromagnet system exhibits off-resonant all-optical switching and our calculations follows the whole state of the system during the switching process including the self consistent determination of the band structure. We stress that the magnetization-switching behavior does not result only for a narrow range of parameters, but is a rather robust phenomenon in our model system. In particular, it does not depend strongly on the detuning in the range of several 10s to about 500 meV.

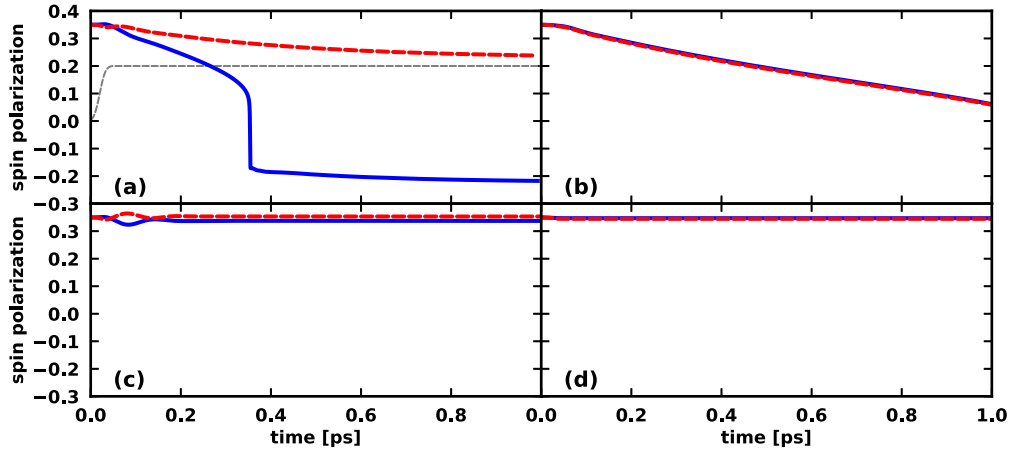

FIG. 5. (a) Time-dependent magnetization (spin polarization) of the ferromagnetic model system excited by a optical field with right-circular (dashed line) and left-circular (solid line) helicity. Magnetization switching occurs only for left-circularly-polarized excitation. (b) without quantum coherence but with scattering, (c) with quantum coherence, no scattering, (d) no quantum coherence, no scattering.

The different magnetization switching behavior for the opposite polarizations must come from those terms in the calculation that arise from including the spin-orbit coupling in the electron bands, in particular the nonvanishing quantum coherence. In the presence of spin-orbit coupling, there is a nonzero contribution to the dynamics of the quantum coherence in Eq. (6), because now terms involving $\Omega_{+,-3/2}$ and $\rho^{-3/2,-}$ are nonzero, which vanish in the case of parabolic bands depicted in Fig. 3. The quantum coherence can be viewed as a dynamical counterpart to the field induced matrix elements calculated by Qaiumzadeh *et al.* In our view, in a dynamical calculation, a more direct interpretation of the influence of the quantum coherence is that it describes a vector component perpendicular to the direction of the k-dependent internal effective magnetic fields, which are present due to the spin-orbit coupling. Tilting the spin out of its equilibrium position at each k point leads to k-resolved precessional dynamics, which can be converted into a change of the ensemble spin (i.e., the magnetization) by combination with a spin-independent scattering process, such as the one described by Eq. (5) [35]. The field-dependent driving terms in Eq. (6) are second order in the optical field and thus contribute after the switching-on dynamics when the field is essentially continuous wave. In addition to the magnetization we also show the total energy density (9) in Fig. 4(b) and the carrier density in the electronic bands in Fig. 4(c). As in the case of Fig. 3, when the optical field is switched on, the energy density increases rapidly, and we see the same behavior for the coherently driving electronic occupations. The increase in energy roughly corresponds to an effective heating. It opens up the scattering phase space that is needed to convert the precessional dynamics into a change of magnetization, which is the microscopic mechanism of change in spin polarization of spin-orbit coupled conduction electrons, as we have shown in Ref. [35]. However, this increase of energy, or "heating" also contributes to a demagnetizing effect, that reduces the magnetization, regardless of the helicity of the optical excitation. The combination of both contributions leads to a steady state. For left circular polarization the heat-induced effect works at first in the same direction as the helicity dependent effect, but after the switching it contributes to demagnetization at later times, which gives rise to a steady state with switched magnetization, that is reduced in magnitude compared to the unexcited system.

C. Influence of the quantum coherence

In Fig. 5, we investigate the influence of the quantum coherence, which is driven in second order of the field. To this end, we show the spin polarization (magnetization) dynamics for different calculations. Figure 5(a) is the same as Fig. 4(a), which results from the full calculation with all microscopic polarizations in Eq. (4), in particular the quantum coherence shown explicitly in Eq. (6) and the scattering contribution (5). In Fig. 5(b), we keep all parameters fixed, but artificially switch off the contributions of the "quantum coherence" to the equations of motion (4) that couple to the E field, i.e. those terms occurring in (6) that are multiplied by Ω s (i.e., the optical field). In the picture of Fig. 1, the coherence ρ^{+-} may still exist due to electronic redistribution in the spin-orbit coupled bands due to Eq. (5), but it is *not driven* by the E field. In this case, no helicity dependent dynamics occur and no switching is achieved, only a comparatively slow demagnetization. As already mentioned in connection with Fig. 4, this is the demagnetizing effect of increasing the electronic energy density, which acts in the same way as heating, and this process leads to spin flips and thus a reduction in the magnetization. The absence of switching in Fig. 5(b) shows that the role of the quantum coherence is crucial for the switching process.

Furthermore, without the quantum coherence, the dynamics for circularly left polarized optical fields and circularly right polarized optical fields are very similar, so that the effect of the light polarization is exclusively due to the quantum coherence. The latter can enhance the heat-induced demagnetization or work against the heat induced effect, as the comparison of the full calculation in Fig. 5(a) with the heating-only calculation in Fig. 5(b) shows. We next turn to Fig. 5(c) where we keep the full quantum coherence dynamics, but set the scattering contribution (5) to zero. In this case,

we find a weak polarization dynamics that does not lead to magnetization switching, but the helicity dependence is more pronounced than in the case of Figs. 3(a) and 5(b) where the field-driven quantum coherence was neglected. Because of the more complicated k-dependent electron-hole transitions in the presence of the Rashba spin-orbit coupling there is an oscillatory behavior and at long times and the helicity dependence is actually opposite to that obtained in Fig. 3, where the Rashba contribution and the field driven quantum coherence was neglected. If one looks closely at the dynamics at early times in Fig. 5, the initial dynamics are in the same direction as in Fig. 3, as the system responds directly to the optical fields. Only after the quantum coherence is driven and starts building up, the spin polarizations are changed in the opposite direction compared to Fig. 3. This again illustrates nicely the influence of the quantum coherence and its role as a supplier of lattice angular momentum to the system. Lastly, Fig. 5(d) serves as a check what happens if we switch off both the field-driven quantum coherence and the scattering contributions. In this case we find only a very weak helicity dependence, comparable to that of Fig. 3(a). In Figs. 5(c) and 5(d), there is no demagnetization due to heating at longer times because there is no scattering that can lead to effective spin flips.

We would like to comment here on the connection to perturbation calculations with respect to the external field, which is often regarded as the contribution of the coherent optical field alone. We have achieved such a setup already in Fig. 5(c) where the magnetization dynamics occurs for an essentially fixed band structure. In this case, the Stoner mean-field splitting is practically constant, so that the change in magnetization comes from the dynamics of the reduced density matrix under the influence of the optical field. In this scenario, depending on the helicity of the optical field, the magnetization approaches different steady states with a magnetization that is changed from its equilibrium value. As the density matrix includes the influence of the coherent field to all orders of the field, this result should correspond to a mechanism for the inverse Faraday effect analyzed by Oppeneer and coworkers in the framework of second-order perturbation theory for close-to-resonance fields. Indeed, Berritta *et al.* [30] have found that the influence of optical fields with opposite circular polarization may lead to a reduced steady-state magnetization. Our result is somewhere in between Ref. [30] and older theories of the inverse Faraday effect for nonmagnetic materials that yielded exactly opposite effective magnetic fields. These should change the magnetization in opposite directions, but with the same magnitude. This "antisymmetry" between the opposite helicities is broken because of the finite equilibrium magnetization. In our case, we find almost the antisymmetry expected for the nonmagnetic materials due to our off-resonant optical field. We have checked that for fields closer to resonance or for larger magnetic splittings we obtain a larger deviation from the perfect antisymmetry.

D. Excitation conditions and model parameters

In this section, we discuss the influence of the excitation conditions and the model parameters on the switching dynamics. In particular, we examine the optical intensity (i.e., Rabi energy), detuning of the optical field with respect to the gap, the Rashba parameter, and the Stoner parameter.

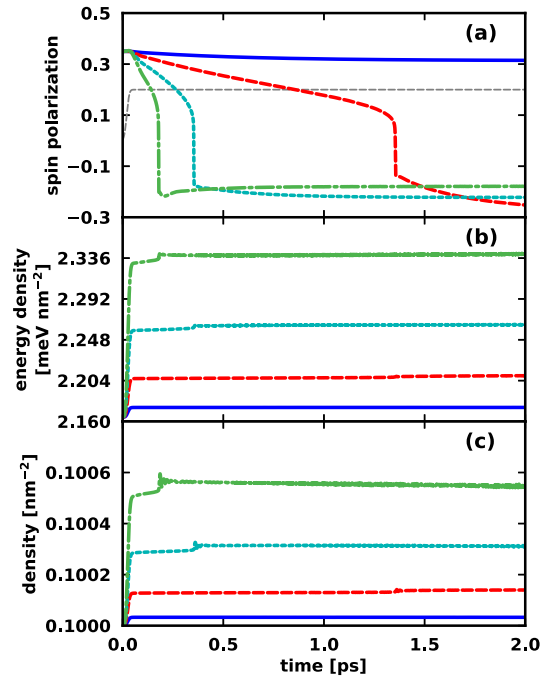

FIG. 6. (a) Spin polarization dynamics for a Rabi energy $\hbar\Omega = 5$ (blue solid line), 10 (red dashed line), 15 (light blue dotted line), and 20 meV (green dash-dotted line) for a circularly left polarized optical field. (b) Corresponding energy density. (c) Corresponding particle density.

We first analyze the influence of the intensity of the optical field for the same detuning and model parameters as above. In Fig. 6, we show the magnetization dynamics, the energy density and the carrier density in the magnetic bands for Rabi energies in the range of 5.0 to 20.0 meV. This figure can be compared to Fig. 4. As the intensity is proportional to the Rabi energy squared, this corresponds to an increase by a factor of 16. The magnetization dynamics results shown in Fig. 6(a) differ in three characteristics: the switching time, which becomes shorter for increasing intensity, the magnitude of the fast switching component, and the long-time behavior of the "switched" magnetization. As Figs. 6(b) and 6(c) show, the larger intensity also leads to an increase in the energy density and density that scales roughly quadratically with Rabi energy (or linearly with intensity). The switching time is determined by an interplay of the increase in energy density and the helicity dependent effect of the optical field. The inreased energy density leads to a stronger initial quenching of the magnetization, and the increased helicity-dependent effect can switch a larger residual magnetization. The latter effect is the reason for the different changes in magnetization that happen during the almost instantaneous switching process. The increase in energy is also responsible for the long-time behavior as the switched magnetization is reached for an system with increased kinetic energy of the electrons for larger Rabi energies, and the increased energy density corresponds to a smaller magnetitude of the magnetization.

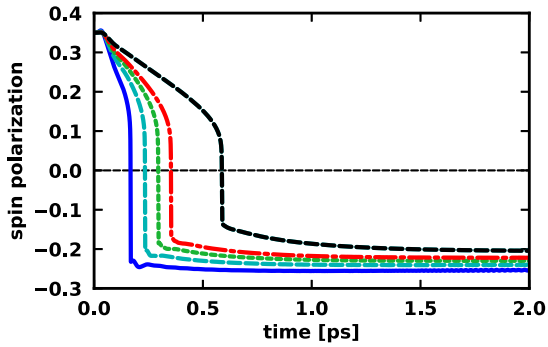

FIG. 7. Spin polarization dynamics a detuning $\delta = 50$, 100, 200, 400, and 800 meV for a circularly left polarized optical field.

In Fig. 7, we investigate the dependence of the magnetization dynamics on the detuning of the off-resonant circularly left polarized optical fields. We increase the detuning over the appreciable range from 50 to 800 meV with respect to a 1.5 eV gap. We find a robust switching scenario that does not strongly depend on the detuning. For smaller detuning, we obtain a faster switching and a larger magnitude of the switched magnetization. In accordance with the discussion above concerning Fig. 6, the smaller detuning leads to an increased energy density and a larger helicity-dependent effect. Also, this combination leads to faster switching times for smaller detuning. We now have a smaller deviation in energy density between the different curves (as compared to Fig. 6, not shown), but we still see a pronounced difference in the helicity dependent effect that determines the almost instantaneous switching process. The smaller increase in energy density does not lead to a reduction of the long-time switched magnetization for closer-to-resonance excitation.

We next examine the switching behavior for different model parameters. In Fig. 8, we display the dependence of the spin polarization/magnetization dynamics for different values of the sRashba parameter. We keep the excitation conditions as in Fig. 4 and change the Stoner parameter such that the equilibrium spin polarization is the same for all configurations. The Stoner parameter is changed by no more than 4%. The magnitude of the Rashba parameter allows us to control the strength of the Rashba SOC in the electronic states, which

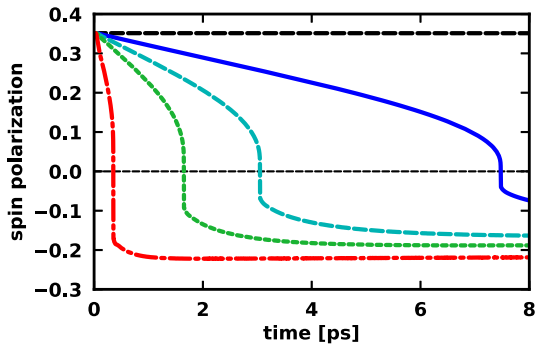

FIG. 8. Spin polarization dynamics for $\alpha = 0$ (black dashed line), 5 (blue solid line), 10 (light blue dashed line), 10 (green dotted line), and 25 meV nm (red dash-dotted line) for a circularly left polarized optical field.

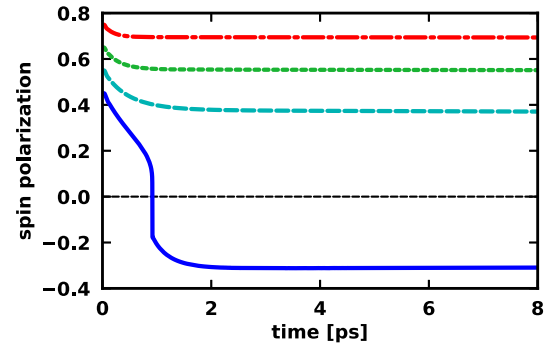

FIG. 9. Spin polarization dynamics for a Stoner parameter $U = 50.8$, 51.8, 53.5, 56.8, and 64.0 meV for a circularly left polarized optical field.

influences the noncollinearity of the electronic spin structure and enhances the dipole transitions associated with the thin lines in Fig. 1. The latter effect means that the optical field can drive the quantum coherence more efficiently, and the former effect means that the magnetization quenching due to the "heating" effect is more pronounced. The connection between magnetization quenching on the one hand and the interplay between precessional dynamics around k-local internal magnetic fields and spin-independent scattering mechanisms has become has been stressed by us earlier [35]. Instead of the microscopic scattering contribution in Ref. [35] we here use a spin-conserving relaxation time ansatz, but this approximation captures the effect on the magnetization dynamics of spin-independent scattering mechanisms quite well. Figure 8 thus shows that the change in Rashba spin-orbit coupling works in the expected way inasmuch as an increase in α leads to a more efficient switching. It shortens the switching time and leads to larger magnitude of the switched magnetization. In case of a vanishing quantum coherence, switching does not occur and the spin polarization dynamics is completely determined by the angular momentum provided by the optical field alone. For large values of α, we do not approach a complete reversal of the magnetization because for two reasons. First, we end up in a state with increased energy density, as discussed above. Second, the α and U parameters are coupled together to ensure the same initial magnetization, but they work in opposite directions as far as the magnetization switching is concerned, as will be discussed next.

Finally, in Fig. 9, we plot the spin polarization/magnetization dynamics for different values of the Stoner parameter U. Here, we keep the excitation conditions as in the previous section and the Rashba parameter fixed at $\alpha = 20$ meV nm. For increasing magnitude of the Stoner parameter U, the magnetic splitting increases, resulting in a larger equilibrium magnetization, as visible in Fig. 9. For increasing Stoner parameter, which is equivalent to an increased magnetic gap in the electronic bands, the switching becomes suppressed so that only demagnetization occurs, and the demagnetization becomes less pronounced with further increase of U. As discussed in connection with Fig. 4 above, the optical field can switch the magnetization only if electronic energy ("heating") is large enough to sufficiently quench the magnetization before the switching occurs, and if the helicity-dependent effect is large enough. For larger magnetic gaps,

a similar electronic excitation will lead to a less pronounced quenching of the magnetization and thus either a less efficient switching process or only to a moderate demagnetization. In addition, electron-electron scattering processes becomes less efficient as the magnetic gap increases because the transfer of momentum and energy between the scattering partners becomes larger, thus leaving few possible scattering channels.

IV. CONCLUSIONS

We introduced a microscopic dynamical model to study the all-optical magnetization switching process in a simple ferromagnetic band structure with a band gap, which includes spin-orbit coupling and incoherent carrier redistribution/scattering processes. As we focus on off-resonant optical excitation with circularly polarized optical fields, we microscopically investigated the IFE in this system. We studied the magnetization dynamics for the case of a ramped-up CW field, and studied the influence of excitation conditions and model parameters that determine the strength of the spin-orbit coupling and ferromagnetic splitting. In our computed magnetization dynamics, we found two contributions. One is connected with the off-resonant analog of the specular IFE effect and the optical spin-transfer torque of Ref. [31]. The other one is due to the quantum coherence (or spin coherence/precession) driven by the optical field, and corresponds to the optical spin-orbit torque of Ref. [31]. In the first contribution, which is responsible for the specular IFE effect, as observed by Zheludev and coworkers in semiconductors, the angular momentum of the field is supplied to the combined system of electrons and holes, thereby changing the spin polarization. For off-resonant excitation, we found that this contribution does not lead to switching, even though it does lead to a helicity-dependent effect on the magnetization, and thus constitutes a microscopic contribution to the IFE.

We found that magnetization switching is a rather robust effect in the present model system and occurs mainly because the optical field drives a quantum coherence between the magnetic bands, i.e., a spin precession around internal spin-orbit fields. Combined with incoherent carrier redistribution/scattering [35] the precessional dynamics changes the magnetization in a polarization dependent way, which leads to magnetization switching due to angular momentum supplied by the lattice, in accordance with Refs. [27,31].

ACKNOWLEDGMENTS

Svenja Vollmar received a fellowship through the Excellence Initiative (DFG/GSC 266). We acknowledge support from DFG by the SFB/TRR 173 Spin+X (Project A08).

[1] I. Radu, K. Vahaplar, C. Stamm, T. Kachel, N. Pontius, H. A. Dürr, T. A. Ostler, J. Barker, R. F. L. Evans, R. W. Chantrell, A. Tsukamoto, A. Itoh, A. Kirilyuk, T. Rasing, and A. V. Kimel, Nature (London) **472**, 205 (2011).

[2] J. H. Mentink, J. Hellsvik, D. V. Afanasiev, B. A. Ivanov, A. Kirilyuk, A. V. Kimel, O. Eriksson, M. I. Katsnelson, and T. Rasing, Phys. Rev. Lett. **108**, 057202 (2012).

[3] T. A. Ostler, J. Barker, R. F. L. Evans, R. W. Chantrell, U. Atxitia, O. Chubykalo-Fesenko, S. El Moussaoui, L. Le Guyader, E. Mengotti, L. J. Heyderman, F. Nolting, A. Tsukamoto, A. Itoh, D. Afanasiev, B. A. Ivanov, A. M. Kalashnikova, K. Vahaplar, J. Mentink, A. Kirilyuk, T. Rasing, and A. V. Kimel, Nat. Commun. **3**, 666 (2012).

[4] S. Wienholdt, D. Hinzke, K. Carva, P. M. Oppeneer, and U. Nowak, Phys. Rev. B **88**, 020406(R) (2013).

[5] A. Baral and H. C. Schneider, Phys. Rev. B **91**, 100402(R) (2015).

[6] S. Mangin, M. Gottwald, C.-H. Lambert, D. Steil, V. Uhlíř, L. Pang, M. Hehn, S. Alebrand, M. Cinchetti, G. Malinowski, Y. Fainman, M. Aeschlimann, and E. E. Fullerton, Nat. Mater. **13**, 286 (2014).

[7] R. John, M. Berritta, D. Hinzke, C. Müller, T. Santos, H. Ulrichs, P. Nieves, J. Walowski, R. Mondal, O. Chubykalo-Fesenko, J. McCord, P. M. Oppeneer, U. Nowak, and M. Münzenberg, Sci. Rep. **7**, 4114 (2017).

[8] A. V. Kimel, A. Kirilyuk, P. A. Usachev, R. V. Pisarev, A. M. Balbashov, and T. Rasing, Nature (London) **435**, 655 (2005).

[9] A. Kirilyuk, A. V. Kimel, and T. Rasing, Rev. Mod. Phys. **82**, 2731 (2010).

[10] Y. K. Takahashi, R. Medapalli, S. Kasai, J. Wang, K. Ishioka, S. H. Wee, O. Hellwig, K. Hono, and E. E. Fullerton, Phys. Rev. Appl. **6**, 054004 (2016).

[11] R. Medapalli, D. Afanasiev, D. K. Kim, Y. Quessab, S. Manna, S. A. Montoya, A. Kirilyuk, T. Rasing, A. V. Kimel, and E. E. Fullerton, Phys. Rev. B **96**, 224421 (2017).

[12] Y. Quessab, R. Medapalli, M. S. El Hadri, M. Hehn, G. Malinowski, E. E. Fullerton, and S. Mangin, Phys. Rev. B **97**, 054419 (2018).

[13] L. P. Pitaevskii, J. Exptl. Theoret. Phys. (U.S.S.R.) **39**, 1450 (1961) [Sov. Phys. JETP **12**, 1008 (1961)].

[14] P. S. Pershan, J. P. van der Ziel, and L. D. Malmstrom, Phys. Rev. **143**, 574 (1966).

[15] R. V. Mikhaylovskiy, E. Hendry, and V. V. Kruglyak, Phys. Rev. B **86**, 100405(R) (2012).

[16] R. Hertel, J. Magn. Magn. Mater. **303**, L1 (2006).

[17] M. I. Kurkin, N. B. Bakulina, and R. V. Pisarev, Phys. Rev. B **78**, 134430 (2008).

[18] R. Hertel and M. Fähnle, Phys. Rev. B **91**, 020411(R) (2015).

[19] S. R. Woodford, Phys. Rev. B **79**, 212412 (2009).

[20] V. N. Gridnev, Phys. Rev. B **88**, 014405 (2013).

[21] K. Taguchi and G. Tatara, Phys. Rev. B **84**, 174433 (2011).

[22] V. M. Edelstein, Phys. Rev. Lett. **80**, 5766 (1998).

[23] A. Qaiumzadeh and M. Titov, Phys. Rev. B **94**, 014425 (2016).

[24] N. I. Zheludev, M. A. Brummell, R. T. Harley, A. Malinowski, S. V. Popov, D. E. Ashenford, and B. Lunn, Solid State Commun. **89**, 823 (1994).

[25] D. Popova, A. Bringer, and S. Blügel, Phys. Rev. B **85**, 094419 (2012).

[26] D. Popova, A. Bringer, and S. Blügel, Phys. Rev. B **84**, 214421 (2011).

[27] A. Qaiumzadeh, G. E. W. Bauer, and A. Brataas, Phys. Rev. B **88**, 064416 (2013).
[28] Y. R. Shen, *The Principles of Nonlinear Optics* (Wiley-Interscience, New York, 1984).
[29] M. Battiato, G. Barbalinardo, and P. M. Oppeneer, Phys. Rev. B **89**, 014413 (2014).
[30] M. Berritta, R. Mondal, K. Carva, and P. M. Oppeneer, Phys. Rev. Lett. **117**, 137203 (2016).
[31] J. Li and P. M. Haney, Phys. Rev. B **96**, 054447 (2017).
[32] V. Shokeen, M. Sanchez Piaia, J.-Y. Bigot, T. Müller, P. Elliott, J. K. Dewhurst, S. Sharma, and E. K. U. Gross, Phys. Rev. Lett. **119**, 107203 (2017).
[33] W. Töws and G. M. Pastor, Phys. Rev. Lett. **115**, 217204 (2015).
[34] A. R. Bungay, S. V. Popov, I. R. Shatwell, and N. I. Zheludev, Phys. Lett. A **234**, 379 (1997).
[35] K. Leckron, S. Vollmar, and H. C. Schneider, Phys. Rev. B **96**, 140408(R) (2017).
[36] H. Haug and S. W. Koch, *Quantum Theory of the Optical and Electronic Properties of Semiconductors*, 5th ed. (World Scientific, Singapore, 2009).
[37] B. Y. Mueller, A. Baral, S. Vollmar, M. Cinchetti, M. Aeschlimann, H. C. Schneider, and B. Rethfeld, Phys. Rev. Lett. **111**, 167204 (2013).
[38] K. Leckron and H. C. Schneider, J. Magn. Magn. Mater. **471**, 482 (2018).
[39] A. R. Khorsand, M. Savoini, A. Kirilyuk, A. V. Kimel, A. Tsukamoto, A. Itoh, and T. Rasing, Phys. Rev. Lett. **108**, 127205 (2012).
[40] M. O. Scully and Z. M, *Quantum Optics* (Cambridge University Press, Cambridge, UK, 1995).
[41] J. Fabian, A. Matos-Abiague, C. Ertler, P. Stano, and I. Zutic, Acta Phys. Slovaca **57**, 565 (2007).
[42] M. S. El Hadri, P. Pirro, C. H. Lambert, S. Petit-Watelot, Y. Quessab, M. Hehn, F. Montaigne, G. Malinowski, and S. Mangin, Phys. Rev. B **94**, 064412 (2016).